Since January 2020 Elsevier has created a COVID-19 resource centre with free information in English and Mandarin on the novel coronavirus COVID-19. The COVID-19 resource centre is hosted on Elsevier Connect, the company's public news and information website.

Bioorganic Chemistry 119 (2022) 105574

Contents lists available at ScienceDirect

Bioorganic Chemistry

journal homepage: www.elsevier.com/locate/bioorg

Virtual screening and *in vitro* validation of natural compound inhibitors against SARS-CoV-2 spike protein

Helen Power [a,b,c], Jiadai Wu [a,b], Stuart Turville [d], Anupriya Aggarwal [d], Peter Valtchev [a,b], Aaron Schindeler [a,b,c], Fariba Dehghani [a,b,*]

[a] School of Chemical and Biomolecular Engineering, Faculty of Engineering, The University of Sydney, Sydney, NSW 2006, Australia
[b] Centre for Advanced Food Engineering, The University of Sydney, Sydney, NSW 2006, Australia
[c] Bioengineering and Molecular Medicine Laboratory, The Children's Hospital at Westmead and Westmead Institute for Medical Research, Westmead, NSW 2145, Australia
[d] The Kirby Institute, University of NSW, Kensington, NSW 2052, Australia

ARTICLE INFO

Keywords:
SARS-CoV-2
COVID-19
Molecular modeling
Virus neutralization assay
Natural compound inhibitor

ABSTRACT

The COVID-19 pandemic caused by the SARS-CoV-2 virus has led to a major public health burden and has resulted in millions of deaths worldwide. As effective treatments are limited, there is a significant requirement for high-throughput, low resource methods for the discovery of novel antivirals. The SARS-CoV-2 spike protein plays a key role in viral entry and has been identified as a therapeutic target. Using the available spike crystal structure, we performed a virtual screen with a library of 527 209 natural compounds against the receptor binding domain of this protein. Top hits from this screen were subjected to a second, more comprehensive molecular docking experiment and filtered for favourable ADMET properties. The *in vitro* activity of 10 highly ranked compounds was assessed using a virus neutralisation assay designed to facilitate viral entry in a physiologically relevant manner *via* the plasma membrane route. Subsequently, four compounds ZINC02111387, ZINC02122196, SN00074072 and ZINC04090608 were identified to possess antiviral activity in the μM range. These findings validate the virtual screening method as a tool for identifying novel antivirals and provide a basis for future drug development against SARS-CoV-2.

1. Introduction

Since its emergence in Wuhan in December 2019, severe acute respiratory syndrome coronavirus 2 (SARS-CoV-2) has become a global health concern. As of July 2021, it has caused over 186 million infections and 4 million deaths [1]. The wild-type virus and its variants are highly transmissible with the potential to rapidly overwhelm healthcare systems [2,3]. The associated illness, known as coronavirus disease (COVID-19) has a wide range of symptoms but is typically associated with fever, cough, fatigue, loss of smell and taste, loss of appetite and muscle pain [4,5]. Serious complications have also been associated with the disease, including clotting disorders, cardiac injury, stroke, and seizures [6–8]. Moreover, long-term symptoms persisting from 3 weeks to months after disease onset occur in 10–30% of patients [9–11], including in patients no longer testing positive for the virus [12].

Since the detection of the initial Wuhan strain, several variants of concern have emerged. In particular, the variants known as alpha, beta, gamma, and delta have spread rapidly and feature mutations associated with increased transmissibility and virulence and the ability to evade the host immune response [13,14]. Currently, only one drug (remdesivir) has been approved by the FDA for non-emergency treatment of COVID-19 [15]. Remdesivir is a repurposed broad-spectrum antiviral that targets viral RNA production [16]. However, results from multiple clinical trials suggest that this drug may not improve mortality or other relevant health outcomes [17]. Monoclonal antibodies against SARS-CoV-2 have also been explored as a treatment option and are currently FDA approved for emergency use only [15]. These treatments including bamlanivimab, etesevimab, casirivimab, imdevimab and sotrovimab, are most effective as an early intervention and are not authorised for patients hospitalised for COVID-19. Moreover, supply limitations and the requirement for mAbs to be administered systemically, prevents the widespread use of these therapies [18,19]. There is also a risk of resistance to common circulating variants, as observed with bamlanivimab, etesevimab and casirivimab [20].

* Corresponding author at: Room 453, School of Chemical and Biomolecular Engineering, Faculty of Engineering, The University of Sydney, Australia.
E-mail address: fariba.dehghani@sydney.edu.au (F. Dehghani).

https://doi.org/10.1016/j.bioorg.2021.105574
Received 17 October 2021; Received in revised form 24 November 2021; Accepted 16 December 2021
Available online 21 December 2021

There is a strong interest in finding rapid and economical methods to identify new and effective anti-coronavirus treatments. Virtual screening involves computational estimation of the optimal binding of a library of potential drugs against targets of interest. This procedure can greatly reduce the time and cost of the drug development compared to *in vitro* screening alone and has been frequently used to identify compounds with therapeutic potential [21–25]. Natural compounds are a valuable source of molecules for drug screening. These represent a diverse range of chemical structures, many with known therapeutic properties. In fact, of the 1328 drugs approved by the US Food & Drug Administration between 1981 and 2016, 41% were natural or derived from natural products [26]. Natural compound libraries offer advantages for drug discovery due to their high structural diversity, a feature necessary for selective and specific interactions with protein targets [27].

For SARS-CoV-2, the viral spike protein represents a key therapeutic target as it mediates viral entry into host cells. The spike protein binds to the cellular receptor angiotensin-converting enzyme 2 (ACE2), leading to spike cleavage by the host enzyme transmembrane serine protease (TMPRSS2) [28]. The structure of the receptor binding domain of the Wuhan strain complexed with ACE2 has since been solved by Lan *et al.* and Shang *et al.* using X-ray crystallography [29,30]. Contacting residues have been identified, including two key regions involved in the stabilisation of the binding interaction. These two regions, known as the Lys31 and Lys353 hotspots, provide a basis for the design of targeted treatments that could prevent the early stages of infection.

Using this information, we aimed to identify natural compounds with anti-SARS-CoV-2 activity using a combined molecular docking and *in vitro* approach. Most docking studies screening natural compounds against the spike protein have screened only a small number of ligands ($\leq$200) and focus on the computational aspect alone [31–40]. Even larger-scale studies do not include experimental validation [41–43]. To address these limitations, we performed a structure-based docking study targeted at the regions of the spike receptor binding domain (RBD) involved in stabilisation of the Lys31 and Lys353 hotspots. A virtual screen against this site was performed with a total of 527 209 molecules from five natural product databases: phenol explorer [44], marine natural products [45], ZINC [46], Super Natural II [47] and the Human Metabolome Database [48]. After filtering top hits for favourable drug-like characteristics, commercially available compounds were validated using a cell model designed to replicate infection in humans. This model uses human embryonic kidney (HEK) cells genetically modified to express ACE2 and TMPRSS2, thus facilitating viral entry in a physiologically relevant manner via the plasma membrane route [28]. Subsequently, we identified four compounds with anti-SARS-CoV-2 activity in the μg/ml range. We also discussed the relevancy of this model in relation to the emerging variants of concern. These findings highlight the capacity of virtual screening to successfully identify inhibitory molecules and provide a basis for further studies regarding viral mechanisms and drug optimisation.

2. Methods

2.1. In silico methods

2.1.1. File preparation and virtual screening strategy

Virtual screening was conducted against the spike protein of SARS-CoV-2 using a library of 527 209 compounds from five natural compound libraries (SuperNatural II, Phenol Explorer, Human Metabolome Database, Marine Natural Products, ZINC Natural Products) available from the Miguel Hernandez University Molecular Docking site (http://docking.umh.es/). Docking was performed using the AutoDock Vina software with a rigid docking protocol [49].

To prepare the protein target for docking, the X-ray derived crystal structure of the SARS-CoV-2 spike receptor-binding domain bound with ACE2 (PDB ID: 6M0J) was downloaded in PDB format from the Research Collaboratory for Structural Bioinformatics Protein Data Bank (https://www.rcsb.org/). PyMOL was used to remove ACE2, water molecules and ions and to add polar hydrogens. The file was then converted to PDBQT format using the PyRx virtual screening tool [50]. The search space of spike was defined to include key regions of the protein involved in the stabilisation of binding to ACE2 (centre: −36.402, 24.771, 6.459; dimensions: 18.703, 29.999, 13.617).

The docking protocol was conducted in two stages. The primary round of screening was performed with all 527 209 ligands. To prepare the ligands for the initial screen, all files were downloaded in SDF format and edited to include polar hydrogens using PyMOL [51]. 3D coordinates were generated by conversion to MOL2 with Marvin Suite 6.0 from ChemAxon [52]. Ligands were then energy minimised and converted to PDBQT format with Open Babel software v 3.1.1 [53]. For the docking of each ligand, the number of docked conformations (modes) and the number of independent runs (exhaustiveness) was set to 10.

To increase the probability of identifying binding conformations with the lowest energy, a secondary round of virtual screening was conducted using the top ligands from the primary screen ranked with the leading 30 scores (n = 12,322). Ligands screened in the second round were energy minimised and converted to PDBQT format using the PyRx virtual screening tool [50]. For this stage, the number of runs was increased to 40.

The binding conformation of the ligands complexed with spike protein were visualised using PyMOL [51]. Residues involved in hydrogen-bonding and hydrophobic interactions were analysed and plotted using the LigPlot^{+} software [54].

2.1.2. ADMET and drug-likeness analysis

To filter compounds with favourable drug-like characteristics, the OSIRIS property explorer was used to calculate the toxicity risk, hydrophilicity (cLogP), solubility (logS), molecular weight (MW), topological surface area (TPSA), drug-likeness and overall drug-score of the top ranked ligands [55]. Compounds with no predicted toxic fragments (mutagenic, tumorigenic, irritant or reproductive effects) and favourable drug-like properties were retained.

2.2. In vitro methods

2.2.1. Chemicals

Ten commercially available compounds with docking scores ≤ -7.9 and favourable drug-like properties were purchased from Vitas-M Laboratory for *in vitro* testing. All compounds were dissolved in DMSO at a concentration of 10 mg/ml and stored at −20 °C.

2.2.2. Cytotoxicity assay

The cytotoxicity of the purchased compounds was initially assessed in VERO cells using the water-soluble tetrazolium salt (WST-1) assay. Twenty-four hours prior to the assay, VERO cells were seeded in 96-well plates at a density of 10,000 cells per well. Cells were then treated with test compounds serially diluted 10-fold to final concentrations of 100 μg/ml, 10 μg/ml, 1 μg/ml, and 0.1 μg/ml. Vehicle controls were prepared by diluting DMSO to final concentrations corresponding to the percentage of DMSO in the prepared chemicals. Untreated cells were prepared as positive controls and wells containing DMEM and DMSO only were used as blanks. Following treatment for 24 h at 37 °C, cells were washed once with DMEM and incubated with 10% WST-1 for 2 h. To determine cell viability, absorbance was measured at 450 nm and 620 nm as a reference wavelength. The relative cell viability was calculated using the following equation:

$$\frac{(A_{450}-A_{620})compounds-(A_{450}-A_{620})blank}{(A_{450}-A_{620})\ no\ treatment\ control-(A_{450}-A_{620})blank}\times 100 = cell\ viability$$

The highest concentration with a cell viability over 75% was selected

as the safe concentration for downstream antiviral assays.

2.2.3. In vitro antiviral activity assay

The human cell line HEK clone 24 used by this study was genetically modified to express ACE2 and TMPRSS2 (PMID:34228725) [56]. Successful genetic modification was assessed based on the ability of this cell line to be infected with a strain of SARS-CoV-2 that is genetically the same as that observed in Wuhan in late 2019 (Clade A2.2).

On the day of the experiment, live HEK-24 cells were stained using NucBlue dye and seeded at 15 k cells per well in a 384-well plate. Dilutions of test compounds were added to cells for 30 min at 37 °C, before an equal volume of virus solution was added. The starting concentration used for each compound was the safe amount determined by the cytotoxicity assay. Each compound was tested at eight concentrations using two-fold serial dilutions in duplicate (n = 2). No virus and virus only conditions were included as controls. Following incubation at 37 °C for 24 h, cells were imaged using the InCell 2500 high throughput microscope (Cytvia). To calculate percentage cell protection, imaged nuclei were quantified using InCarta high-content image analysis software (Cytvia). Virus neutralisation was calculated using the following formula:

$$\%\ neutralisation = [D - \left(1 - \frac{nuclei\ in\ test\ well}{nuclei\ in\ uninfected\ controls}\right).] \times \frac{100}{D}$$

where D represents the percentage of cell death in the absence of test compounds and is calculated as:

$$D = 1 - \frac{nuclei\ in\ virus\ only\ controls}{nuclei\ in\ uninfected\ controls}$$

2.2.4. Statistical analysis

All statistical analyses were performed using the GraphPad Prism 9 software (GraphPad Software, Inc.). Non-linear regression analysis was used to generate dose–response curves and calculate EC_{50} values. Values are represented as the mean ± standard deviation (SD).

3. Results and discussion

3.1. In silico analysis

AutoDock Vina was used to perform molecular docking with a total of 527 209 ligands from five natural compound libraries (SuperNatural II, Phenol Explorer, Human Metabolome Database, Marine Natural Products, ZINC Natural Products). Vina utilises a semi-empirical scoring function based on experimental receptor-ligand conformations and affinities. The docking score generated by Vina accounts for the contribution of steric interactions, hydrophobic interactions and hydrogen bonds and is given as a measure of the Gibbs free energy of the binding interaction. Therefore, the more negative the score, the more favourable the interaction. The top 30 scores from the primary screen ranged from −4.6 to −8.1 and included 12,322 (2.3%) of ligands. A secondary screen to refine the top ligands produced scores ranging from −4.6 to −8.9, with the top 1.0% of ligands (n = 128) scoring ≤ −7.9. A flowchart of the workflow is shown in Fig. 1.

The top 128 ligands were then filtered for commercial availability and adsorption, distribution, metabolism, excretion and toxicity (ADMET) predictors using the OSIRIS property explorer [55]. This software predicts the suitability of a small molecule to function as a drug based on the properties of currently traded drugs and toxicity data from the Registry of Toxic Effects of Chemical Substances (RTECS) database. The calculated properties were toxicity risk (mutagenicity, tumorigenicity, irritating effects and reproductive effects), MW, hydrophilicity (cLogP), solubility (logS), topological polar surface area (TPSA), drug-likeness and overall drug-score cLogP (hydrophilicity), logS (solubility). Of the top 128 ligands, 22 could not be purchased from commercial vendors and a further 25 had limited availability. Of the remaining 81 compounds, 10 had pharmacokinetic profiles aligned with traded drugs (Table 1, Fig. 2). The properties for these 10 compounds ranged from

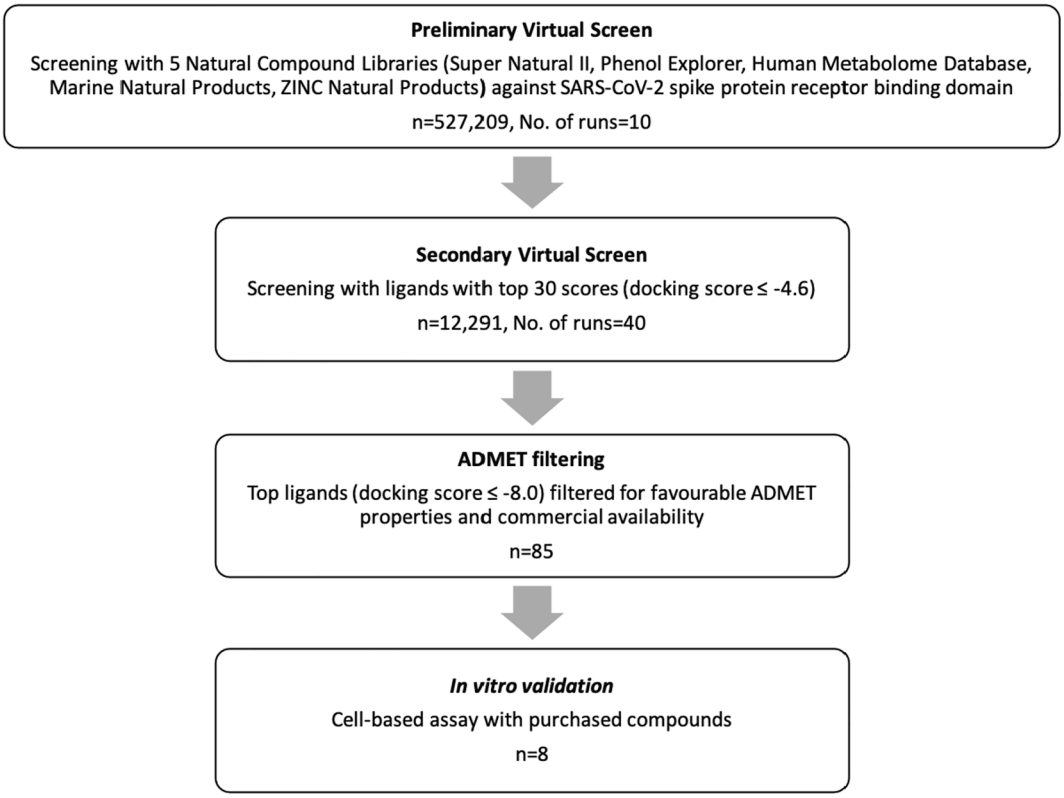

Fig. 1. The workflow for identifying natural compound inhibitors of SARS-CoV-2.

Table 1
ADMET Properties of the top 10 lead compounds from the virtual screen after filtering for commercial availability and suitable pharmacokinetic profiles.

Database ID	Chemical Name	MW (Da)	cLogP	LogS	TPSA (Å^2)	Druglikeness	Drug-score
ZINC02726715	9,10-dimethoxy-2-(naphthalen-2-yloxy)-6,7-dihydro-4H-pyrimido[6,1-*a*]isoquinolin-4-one	400.4	4.33	−5.49	60.4	3.62	0.50
ZINC02122196	(12aS)-2-benzyl-6-(2-methylphenyl)-2,3,6,7,12,12a-hexahydropyrazino[1′,2′:1,6]pyrido[3,4-b]indole-1,4-dione	435.5	1.28	−4.57	58.4	6.64	0.58
ZINC96115460	2-hydroxy-3-[2-oxo-2-(1,3,4,5-tetrahydro-2H-pyrido[4,3-*b*]indol-2-yl)ethyl]-3,4-dihydro-5H-1,4-benzodiazepin-5-one	388.4	1.28	−3.78	94.3	7.76	0.78
SN00074072	(2Z)-1-(1-benzofuran-2-yl)-2-(7,8-dihydro[1,3]dioxolo[4,5-g]isoquinolin-5(6H)-ylidene)ethanone	333.1	3.78	−5.61	60.7	3.85	0.58
ZINC02111387	(12aS)-2-cycloheptyl-6-(3-methoxyphenyl)-2,3,6,7,12,12a-hexahydropyrazino[1′,2′:1,6]pyrido[3,4-b]indole-1,4-dione	457.6	4.11	−4.78	65.6	0.70	0.45
ZINC96114431	[1-(9H-purin-6-yl)piperidin-4-yl](1,3,4,9-tetrahydro-2H-beta-carbolin-2-yl)methanone	401.5	1.98	−4.67	93.8	5.63	0.68
SN00092464	(8S,8aR,11aS)-10-(1,3-benzodioxol-5-ylmethyl)-8-(phenylcarbonyl)-11a,11b-dihydro-8H-pyrrolo[3′,4′ :3,4]pyrrolo[2,1-a]isoquinoline-9,11(8aH,10*H*)-dione	478.5	3.07	−5.50	76.2	4.68	0.50
ZINC04090608	(2Z)-2-(7,8-dihydro[1,3]dioxolo[4,5-g]isoquinolin-5(6H)-ylidene)-1-phenylethanone	293.3	3.27	−4.43	47.6	2.49	0.70
ZINC06624435	(1S,5R)-3-{[(2-oxo-2H-chromen-7-yl)oxy]acetyl}-1,2,3,4,5,6-hexahydro-8H-1,5-methanopyrido[1,2-a][1,5]diazocin-8-one	392.4	1.55	−2.93	76.2	−0.16	0.61
ZINC85878555	3-{[1-(1H-indazol-3-yl)-5-oxopyrrolidin-3-yl]carbonyl}-1,2,3,4,5,6-hexahydro-8H-1,5-methanopyrido[1,2-a][1,5]diazocin-8-one	417.5	1.13	−3.32	89.6	5.61	0.79

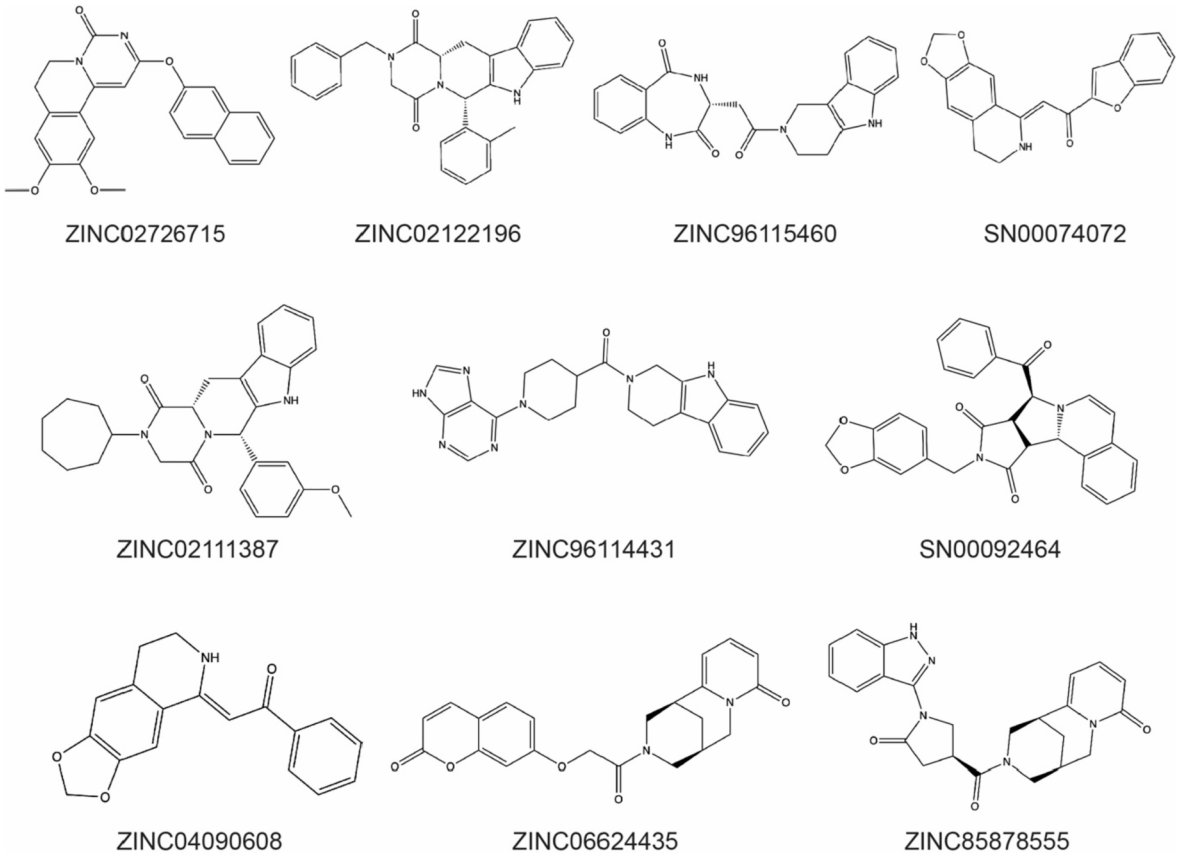

Fig. 2. Structural formulas of the top 10 lead compounds from the virtual screen after filtering for commercial availability and suitable ADMET profiles.

293.3 to 478.5 Da (MW), 1.13–4.33 (cLogP), (−5.61)- (−2.93) (LogS), 47.58–94.3 Å^2 (TPSA), (−0.16)-7.76 (druglikeness) and 0.45–0.79 (drug-score). All compounds had no predicted toxicity risks.

The docking scores for these top 10 compounds ranged from (−8.4)–(−7.9). One ligand had the top docking score of −8.4 (ZINC02726715), two ligands had a docking score of −8.3 (ZINC02122196, ZINC96115460), three ligands had a docking score of −8.1 (SN00074072, ZINC02111387, ZINC96114431) two ligands had a docking score of −8.0 (SN00092464, ZINC04090608) and two ligands had a docking score of −7.9 (ZINC06624435, ZINC85878555). The number of receptor residues involved in the binding interaction ranged from 7 to 11 and the number of hydrogen bonds ranged from 0 to 4 (Table 2). Additionally, all selected compounds contained 4–7 ring structures (Fig. 2). This feature is particularly notable for inhibitors of protein–protein interactions (iPPI), as iPPIs are associated with a greater number of aromatic rings than other drugs [57].

The search space used in the docking study was defined to include the spike residues involved in binding to two key regions of the ACE2 protein known as the Lys31 and Lys353 hotspots. Neutralisation of these lysine residues is required to stabilise the binding interaction between the viral RBD and its receptor. Within the spike protein, Leu455 and Gln493 are required for stabilisation of the Lys31 hotspot and Gly496

Table 2
Molecular docking scores and interacting residues of the top 10 commercially available lead compounds with suitable ADMET profiles.

Database ID	Docking Score	No. of Interacting Residues	No. of H-bonds	Interacting Residues
ZINC02726715	−8.4	11	3	Arg403, **Tyr449**, **Tyr453**, Gln493, Ser494, Tyr495, Gly496, **Gln498**, Asn501, Gly502, Tyr505
ZINC02122196	−8.3	10	1	Arg403, Tyr449, Tyr453, **Ser494**, Tyr495, Gly496, Gln498, Asn501, Gly502, Tyr505
ZINC96115460	−8.3	11	2	Arg403, **Tyr453**, Leu455, Phe456, Glu484, Tyr489, Gln493, Tyr495, Gly496, Asn501, Tyr505
SN00074072	−8.1	7	1	**Tyr453**, Ser494, Tyr495, Gly496, Asn501, Gly502, Tyr505
ZINC02111387	−8.1	11	1	**Arg403**, Lys417, Tyr449, Tyr453, Leu455, Gln493, Ser494, Tyr495, Gly496, Asn501, Tyr505
ZINC96114431	−8.1	9	0	Arg403, Glu406, Tyr453, Ser494, Tyr495, Gly496, Asn501, Gly502, Tyr505
SN00092464	−8.0	10	2	**Arg403**, Glu406, **Tyr453**, Leu455, Gln493, tyr495, Gly496, Phe497, Asn501, Tyr505
ZINC04090608	−8.0	7	2	**Tyr453**, Ser494, Tyr495, **Gly496**, Asn501, Gly502, Tyr505
ZINC06624435	−7.9	8	1	Arg403, Tyr453, Ser494, Tyr495, Gly496, Asn501, **Gly502**, Tyr505
ZINC85878555	−7.9	8	4	Tyr449, **Gln493**, **Ser494**, Tyr495, **Gly496**, **Gln498**, Asn501, Tyr505

Bolded residues are involved in hydrogen bonding.

and Asn501 are required for stabilisation of the Lys353 hotspot [30]. Lys417 forms two salt bridges with ACE2 and is also important for receptor binding [29]. Therefore, the interaction of small molecules with these residues may interfere with stable receptor binding and reduce viral entry. Notably, the docking conformation of all 10 ligands included interactions with both Gly496 and Asn501. Three ligands interacted with Leu455, five ligands interacted with Gln493 and one ligand interacted with Lys417. However, of these 29 interactions with key residues, only three involved hydrogens bonds, with the remaining 26 forming hydrophobic contacts. One compound, ZINC02111387 interacted with all five key residues (Fig. 3, Table 2).

An advantage of molecular docking is the ability of this method to predict the effect of viral mutations on the binding conformation of lead compounds. Changes to residues in the RBD may decrease or increase binding affinity and may also change the structural conformation of the entire domain.

The four main variants of concern: alpha, beta, gamma, and delta, contain mutations in five amino acid residues found in the spike RBD (Fig. 4)[14]. The N501Y mutation has evolved independently in the alpha, beta and gamma variants and has been shown to affect the structural conformation of the RBD and increase binding affinity to ACE2. Notably, Asn501 has been identified in stabilisation of the Lys353 hotspot and as mentioned above, it is predicted to interact with all 10 lead compounds. All variants of concern carry a mutation in Glu484, which is only predicted to interact with ZINC96115460 and two variants, alpha and beta contain a mutation in Lys417, which is only predicted to interact with ZINC02111387. The two mutations unique to the delta variant, L452R and T478K, are not present in any of the interactions. To provide a better prediction of how these mutations may affect binding to specific compounds, further modelling is required, although this depends on the availability of high-resolution protein structures. Currently, molecular structures of the spike protein have been solved by cryo-electron microscopy for the alpha, beta and gamma variants [58]. However, the delta variant spike structure has not yet been solved and high resolution (<2.5 Å) X-ray crystallography structures are currently not available for any variants.

Several approaches may be considered to expand the number of candidate compounds identifiable using computational methods. Firstly, screening larger compound libraries has been shown to increase the number of true-positive hits within the top ranked ligands [59]. However, this requires access to large amounts of computational resources and relies on the availability of extensive compound libraries. When focusing on natural products, even the largest collections contain only hundreds of thousands of molecules [60], compared to other synthetic libraries with over one billion compounds [61]. Another approach is to reduce stringency when filtering for drug-like properties or to eliminate this step entirely. This approach, however, may increase the presence of undesirable properties in lead compounds including poor bioavailability and high cytotoxicity and hence may require further research into appropriate delivery methods or modification of functional groups using techniques such as bioisosterism.

3.2. *In vitro analysis*

The top 10 ranked ligands from the virtual screen that were both commercially available and had favourable ADMET profiles were purchased for *in vitro* assessment of their anti-SARS-CoV-2 activity. The concentration of these compounds employed in antiviral assays was guided by the outcomes of a cytotoxicity assay; this was defined as 100 μg/ml or the highest concentration in which cell viability was over 75%. The highest tested concentration of 100 μg/ml showed >75% viability for six compounds, 10 μg/ml showed >75% viability for three compounds, and 0.1 μg/ml showed >75% viability for one compound (Table 3).

A SARS-CoV-2 infection assay in HEK-24 cells genetically modified to express ACE2 and TMPRSS2 was used to assess the candidate natural compounds. Due to the expression of the TMPRSS2 protease in the human respiratory tract, viral particles largely utilise the plasma membrane route for entry into these tissues. Some alternative cell lines such as VeroE6, do not express the required proteases and entry is predominantly endosomal [28,62]. Therefore, based on physiological relevance, the genetically modified HEK-24 cell line was selected for experimental validation. Using this *in vitro* model, anti-SARS-CoV-2 activity was exhibited by ZINC02111387, ZINC02122196, SN00074072 (maximal dose 100 μg/ml) and ZINC04090608 (maximal dose 10 μg/ml) (Fig. 5, Table 3). ZINC02111387 demonstrated the most potent antiviral activity, neutralising 40.3% of virus at 100 μg/ml and exhibiting an EC_{50} value of 1.12 μg/ml. The other active compounds ZINC02122196, SN00074072 and ZINC04090608, demonstrated 29.8%, 24.9% and 18.3% virus inhibition at their highest tested concentrations respectively. EC_{50} values could not be calculated for these compounds due to the absence of a sigmoidal dose response curve. A dose response may be observable at higher test concentrations, although these were not

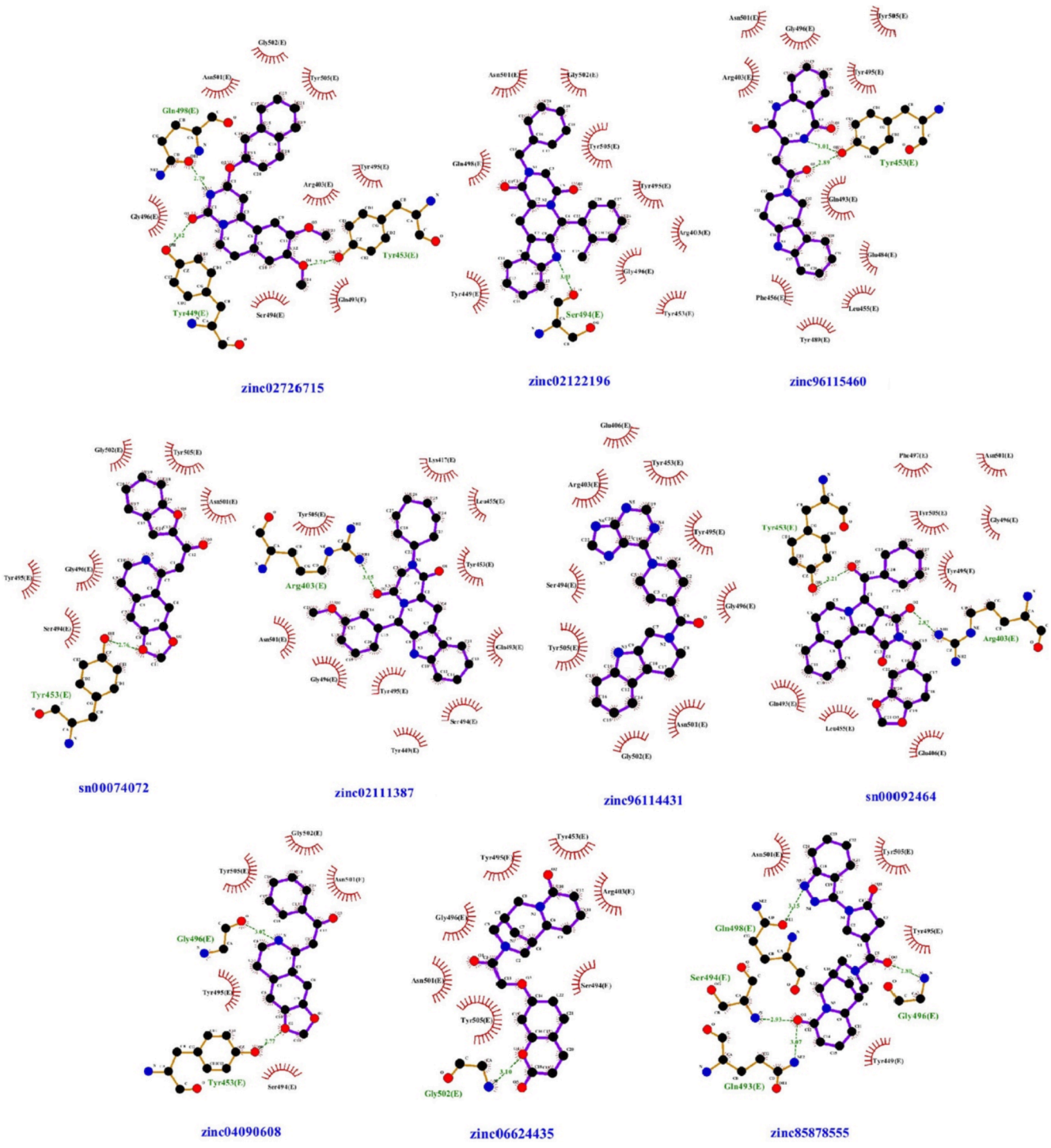

Fig. 3. Interaction diagrams of the top 10 lead compounds from the virtual screen filtered for commercial availability and suitable ADMET profiles. Diagrams were generated using LigPlot^{+} software. Ligand bonds are drawn in purple, receptor bonds are drawn in brown, red lines represent hydrophobic contacts and broken green lines represent hydrogen bonds with distances in Angstroms. (For interpretation of the references to colour in this figure legend, the reader is referred to the web version of this article.)

investigated due to predicted cytotoxicity. The inhibition seen with SN00074072 was not dose responsive; virus neutralisation ranged from 11.3 to 24.8% for all tested concentrations (0.78–100 μg/ml), suggesting that maximum activity has been reached in the low μg/ml range.

For the four compounds that were inhibitory for SARS-CoV-2, docking scores ranged from (−8.3)–(−8.0), the number of predicted interacting residues in the spike protein ranged from 7 to 11, and the number of hydrogen bonds formed ranged from 1 to 2. Notably, the most potent compound ZINC02111387, was predicted to interact with all five key spike residues identified as important for binding to the native ACE2 receptor (Lys417, Leu455, Gln493, Gly496 and Asn501). The remaining three compounds were predicted to interact with two key residues, Gly496 and Asn501. Although there was no calculable association between docking score and virus neutralisation, the two lowest scoring compounds ZINC06624435 and ZINC85878555 did not exhibit any antiviral activity.

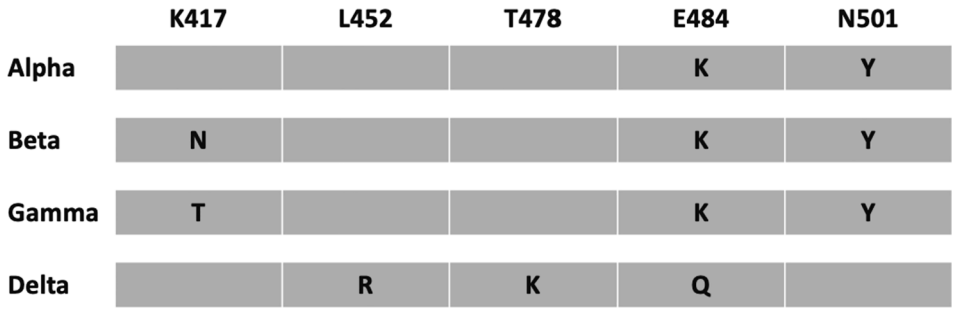

Fig. 4. Mutations in the receptor binding domain of spike protein for the four variants of concern: alpha, beta, gamma and delta.

Table 3
Viral neutralisation of 10 predicted anti-SARS-CoV-2 compounds.

Database ID	Docking Score	Highest tested concentration (μM)	Inhibition (%) at highest concentration
Tested at 100 μg/ml			
ZINC02122196	−8.3	229.6	29.8
SN00074072	−8.1	300.2	24.9
ZINC02111387	−8.1	218.5	40.3
SN00092464	−8.0	209.0	no antiviral activity
ZINC06624435	−7.9	254.8	no antiviral activity
ZINC85878555	−7.9	239.5	no antiviral activity
Tested at 10 μg/ml			
ZINC02726715	−8.4	25.0	no antiviral activity
ZINC04090608	−8.0	34.1	18.3
ZINC96114431	−8.1	24.9	no antiviral activity
Tested at 1 μg/ml			
ZINC96115460	−8.3	2.6	no antiviral activity

The modest number of compounds tested *in vitro* reflects the low off-the-shelf availability of natural compounds with drug-like ADMET profiles. Natural products are advantageous for drug discovery due to their known ability to carry out diverse functions in biological systems and their exceptional structural diversity which is often not observed in large chemical databases [63]. However, many natural compounds are not readily available and if not manufactured synthetically, may require complex extraction and purification procedures. Curation of large-scale purchasable natural product libraries would allow for a greater number of top ranked ligands to be tested *in vitro* and hence increase the probability of identifying antiviral compounds. The structural diversity of natural compounds also results in these molecules exhibiting unique chemical properties which can lead to their removal by traditional filtering methods that focus on ADMET profiles of current drugs, such as Lipinski's rule of five.

Whilst only 10 ligands were tested *in vitro*, four active compounds against SARS-CoV-2 were identified. These experimental results support the suitability of the docking approach used. Previous large-scale docking studies of 69,000–150,000,000 compounds have reported hit rates of 11–41% [64]. Many factors can influence the success of such studies including availability of high-resolution crystal structures for the target protein, presence of co-factors that mediate ligand binding, presence of protein post-translational modifications and the flexibility, size and composition of the targeted binding site. For example, docking against enclosed binding pockets is usually more successful compared to docking against larger, flat and solvent-exposed regions [64].

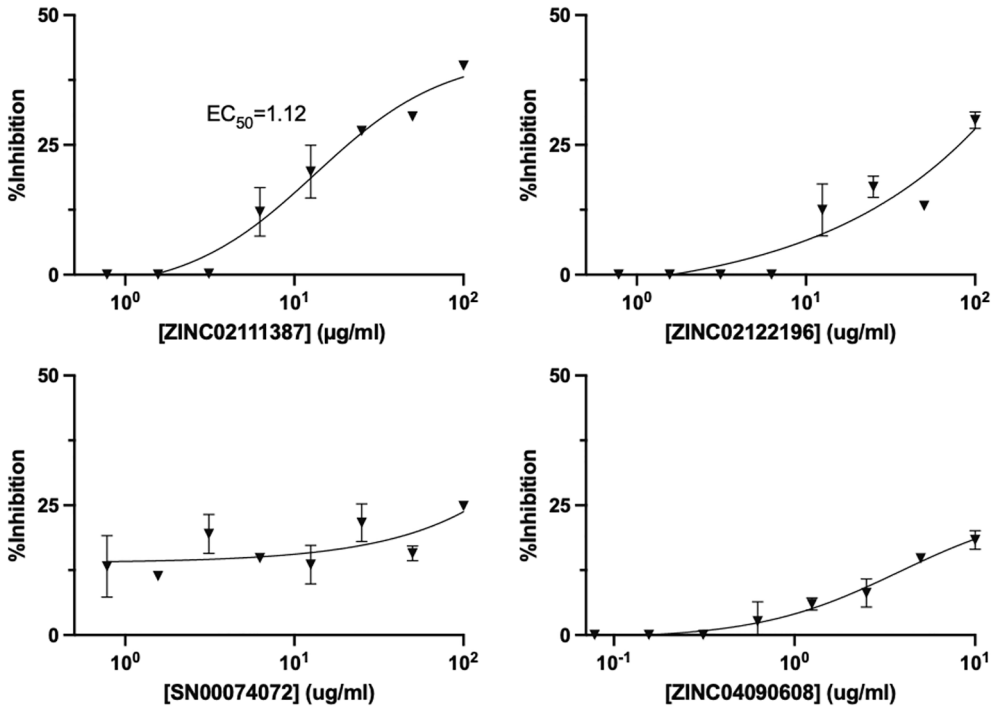

Fig. 5. SARS-CoV-2 inhibition activity of compounds identified through virtual screening. ZINC02111387, ZINC02122196, SN00074072 at 100 μg/ml and ZINC04090608 at 10 μg/ml were serially diluted 2-fold eight times and incubated with HEK-24 cells for 30mins before addition SARS-CoV-2. Following infection for 24 h, cell survival was quantified using microscope imaging of nuclei stained with NucBlue. Data are presented as the mean ± SD of duplicates (n = 2).

Though the antiviral activity of four compounds was confirmed experimentally, validation of the binding mechanism cannot be determined from the virus neutralisation assay. Whilst molecular docking provides a prediction of the binding conformation, viral inhibition may potentially occur through allosteric effects or interactions with biomolecules other than spike. Additional techniques are required to validate the docked conformation, such as SPR for investigating binding kinetics and cryo-electron microscopy or X-ray co-crystallography for analysis of the interaction at an atomic level. From a treatment perspective, however, viral neutralisation assays provide a better indication of drug efficacy in a biological system. Although beyond the scope of this study, further research into the binding mechanism of the anti-SARS-CoV-2 compounds may help to identify key spike residues for drug targeting and to serve as the basis for designing chemical modifications to improve the activity of these compounds.

4. Conclusions

This study demonstrates the ability of a targeted structure-based molecular docking approach combined with *in vitro* validation for the identification of novel antiviral drugs. Despite testing a limited number of compounds *in vitro* (n = 10), we were able to identify four compounds with previously unknown activity against SARS-CoV-2. These active compounds showed 18–40% viral inhibition using an established live virus infection assay. While their activity is low when compared to neutralising antibodies (which have been shown to inhibit 100% of viral particles in the nM range [65]), it nonetheless supports our modelling approach and its capacity to identify compounds with binding affinity to the target site. It may be possible to further augment the binding affinity and antiviral activity of these candidates by targeted chemical modification (bioisosterism), although this is beyond the scope of this modelling project.

Declaration of Competing Interest

The authors declare that they have no known competing financial interests or personal relationships that could have appeared to influence the work reported in this paper.

Acknowledgement

The authors acknowledge the technical assistance of Nathaniel Butterworth of the Sydney Informatics Hub, a Core Research Facility of the University of Sydney and the use of University of Sydney's high performance computing cluster, Artemis.

This research/project was also undertaken with the assistance of the high-performance computing system Gadi from the National Computational Infrastructure (NCI), which is supported by the Australian Government.

Investigators J Wu and H Power received salary support from JAT Energy (Toorak, VIC, Australia).

References

[1] Weekly epidemiological update on COVID-19 – 13 July 2021, in: Emergency Situational Updates, World Health Organisation, 2021.
[2] T.L. Dao, V.T. Hoang, P. Colson, J.C. Lagier, M. Million, D. Raoult, A. Levasseur, P. Gautret, SARS-CoV-2 infectivity and severity of COVID-19 according to SARS-CoV-2 variants: current evidence, J. Clin. Med. 10 (12) (2021) 2635, https://doi.org/10.3390/jcm10122635.
[3] S. Sanche, Y.T. Lin, C. Xu, E. Romero-Severson, N. Hengartner, R. Ke, High contagiousness and rapid spread of severe acute respiratory syndrome coronavirus 2, Emerg. Infect. Dis. 26 (7) (2020) 1470–1477, https://doi.org/10.3201/eid2607.200282.
[4] M.C. Grant, L. Geoghegan, M. Arbyn, Z. Mohammed, L. McGuinness, E.L. Clarke, R. G. Wade, J.A. Hirst, The prevalence of symptoms in 24,410 adults infected by the novel coronavirus (SARS-CoV-2; COVID-19): a systematic review and meta-analysis of 148 studies from 9 countries, PLoS ONE 15 (6) (2020) e0234765, https://doi.org/10.1371/journal.pone.0234765.
[5] C. Menni, A.M. Valdes, M.B. Freidin, C.H. Sudre, L.H. Nguyen, D.A. Drew, S. Ganesh, T. Varsavsky, M.J. Cardoso, J.S. El-Sayed Moustafa, A. Visconti, P. Hysi, R.C.E. Bowyer, M. Mangino, M. Falchi, J. Wolf, S. Ourselin, A.T. Chan, C.J. Steves, T.D. Spector, Real-time tracking of self-reported symptoms to predict potential COVID-19, Nat. Med. 26 (7) (2020) 1037–1040, https://doi.org/10.1038/s41591-020-0916-2.
[6] A.N. Kochi, A.P. Tagliari, G.B. Forleo, G.M. Fassini, C. Tondo, Cardiac and arrhythmic complications in patients with COVID-19, J. Cardiovasc. Electrophysiol. 31 (5) (2020) 1003–1008, https://doi.org/10.1111/jce.14479.
[7] F.A. Klok, M.J.H.A. Kruip, N.J.M. van der Meer, M.S. Arbous, D.A.M.P.J. Gommers, K.M. Kant, F.H.J. Kaptein, J. van Paassen, M.A.M. Stals, M.V. Huisman, H. Endeman, Incidence of thrombotic complications in critically ill ICU patients with COVID-19, Thromb. Res. 191 (2020) 145–147, https://doi.org/10.1016/j.thromres.2020.04.013.
[8] M. Sharifian-Dorche, P. Huot, M. Osherov, D. Wen, A. Saveriano, P.S. Giacomini, J. P. Antel, A. Mowla, Neurological complications of coronavirus infection; a comparative review and lessons learned during the COVID-19 pandemic, J. Neurol. Sci. 417 (2020) 117085, https://doi.org/10.1016/j.jns.2020.117085.
[9] F. Salamanna, F. Veronesi, L. Martini, M.P. Landini, M. Fini, Post-COVID-19 syndrome: the persistent symptoms at the post-viral stage of the disease. A systematic review of the current data, Front. Med. (Lausanne) 8 (2021) 653516, https://doi.org/10.3389/fmed.2021.653516.
[10] S. Bliddal, K. Banasik, O.B. Pedersen, J. Nissen, L. Cantwell, M. Schwinn, M. Tulstrup, D. Westergaard, H. Ullum, S. Brunak, N. Tommerup, B. Feenstra, F. Geller, S.R. Ostrowski, K. Grønbæk, C.H. Nielsen, S.D. Nielsen, U. Feldt-Rasmussen, Acute and persistent symptoms in non-hospitalized PCR-confirmed COVID-19 patients, Sci. Rep. 11 (1) (2021), https://doi.org/10.1038/s41598-021-92045-x.
[11] J.K. Logue, N.M. Franko, D.J. McCulloch, D. McDonald, A. Magedson, C.R. Wolf, H. Y. Chu, Sequelae in adults at 6 months after COVID-19 infection, JAMA Netw. Open 4 (2) (2021) e210830, https://doi.org/10.1001/jamanetworkopen.2021.0830.
[12] A. Carfì, R. Bernabei, F. Landi, Persistent symptoms in patients after acute COVID-19, JAMA 324 (6) (2020) 603, https://doi.org/10.1001/jama.2020.12603.
[13] J. Khateeb, Y. Li, H. Zhang, Emerging SARS-CoV-2 variants of concern and potential intervention approaches, Crit. Care 25 (1) (2021) 244, https://doi.org/10.1186/s13054-021-03662-x.
[14] M.Z. Salleh, J.P. Derrick, Z.Z. Deris, Structural evaluation of the spike glycoprotein variants on SARS-CoV-2 transmission and immune evasion, Int. J. Mol. Sci. 22 (14) (2021) 7425, https://doi.org/10.3390/ijms22147425.
[15] FDA, Coronavirus (COVID-19) | Drugs. Emergency Preparedness | Drugs, 2021 (cited 2021 19th July). Available from: www.fda.gov/drugs/emergency-preparedness-drugs/coronavirus-covid-19-drugs.
[16] A.J. Brown, J. Won, R.L. Graham, K.H. Dinnon, A. Sims, J.Y. Feng, T. Cihlar, M. R. Denison, R.S. Baric, T.P. Sheahan, Broad spectrum antiviral remdesivir inhibits human endemic and zoonotic deltacoronaviruses with a highly divergent RNA dependent RNA polymerase, Antiviral Res. 169 (2019) 104541, https://doi.org/10.1016/j.antiviral.2019.104541.
[17] WHO, Therapeutics and COVID-19: living guideline, 17 December 2020, 2020 [cited 2021 19th July]. Available from: https://apps.who.int/iris/handle/10665/337876.
[18] P.C. Taylor, A.C. Adams, M.M. Hufford, I. de la Torre, K. Winthrop, R.L. Gottlieb, Neutralizing monoclonal antibodies for treatment of COVID-19, Nat. Rev. Immunol. 21 (6) (2021) 382–393, https://doi.org/10.1038/s41577-021-00542-x.
[19] A. Casadevall, E. Dadachova, L.-A. Pirofski, Passive antibody therapy for infectious diseases, Nat. Rev. Microbiol. 2 (9) (2004) 695–703, https://doi.org/10.1038/nrmicro974.
[20] P. Wang, M.S. Nair, L. Liu, S. Iketani, Y. Luo, Y. Guo, M. Wang, J. Yu, B. Zhang, P. D. Kwong, B.S. Graham, J.R. Mascola, J.Y. Chang, M.T. Yin, M. Sobieszczyk, C. A. Kyratsous, L. Shapiro, Z. Sheng, Y. Huang, D.D. Ho, Antibody resistance of SARS-CoV-2 variants B.1.351 and B.1.1.7, Nature 593 (7857) (2021) 130–135, https://doi.org/10.1038/s41586-021-03398-2.
[21] S. Schmidl, O. Ursu, C.V. Iancu, M. Oreb, T.I. Oprea, J.-Y. Choe, Identification of new GLUT2-selective inhibitors through in silico ligand screening and validation in eukaryotic expression systems, Sci. Rep. 11 (1) (2021), https://doi.org/10.1038/s41598-021-93063-5.
[22] Z.P. Lin, N.N. Al Zouabi, M.L. Xu, N.E. Bowen, T.L. Wu, E.S. Lavi, P.H. Huang, Y.-L. Zhu, B. Kim, E.S. Ratner, In silico screening identifies a novel small molecule inhibitor that counteracts PARP inhibitor resistance in ovarian cancer, Sci. Rep. 11 (1) (2021), https://doi.org/10.1038/s41598-021-87325-5.
[23] M. Awasthi, S. Singh, V.P. Pandey, U.N. Dwivedi, Alzheimer's disease: An overview of amyloid beta dependent pathogenesis and its therapeutic implications along with in silico approaches emphasizing the role of natural products, J. Neurol. Sci. 361 (2016) 256–271, https://doi.org/10.1016/j.jns.2016.01.008.
[24] S. Ferla, N.E. Netzler, S. Ferla, S. Veronese, D.E. Tuipulotu, S. Guccione, A. Brancale, P.A. White, M. Bassetto, In silico screening for human norovirus antivirals reveals a novel non-nucleoside inhibitor of the viral polymerase, Sci. Rep. 8 (1) (2018), https://doi.org/10.1038/s41598-018-22303-y.
[25] V. Katritch, V.-P. Jaakola, J.R. Lane, J. Lin, A.P. IJzerman, M. Yeager, I. Kufareva, R.C. Stevens, R. Abagyan, Structure-based discovery of novel chemotypes for adenosine A(2A) receptor antagonists, J. Med. Chem. 53 (4) (2010) 1799–1809, https://doi.org/10.1021/jm901647p.
[26] D.J. Newman, G.M. Cragg, Natural products as sources of new drugs from 1981 to 2014, J. Nat. Prod. 79 (3) (2016) 629–661, https://doi.org/10.1021/acs.jnatprod.5b01055.

[27] W.R. Galloway, A. Isidro-Llobet, D.R. Spring, Diversity-oriented synthesis as a tool for the discovery of novel biologically active small molecules, Nat. Commun. 1 (2010) 80, https://doi.org/10.1038/ncomms1081.

[28] M. Hoffmann, H. Kleine-Weber, S. Schroeder, N. Krüger, T. Herrler, S. Erichsen, T. S. Schiergens, G. Herrler, N.-H. Wu, A. Nitsche, M.A. Müller, C. Drosten, S. Pöhlmann, SARS-CoV-2 cell entry depends on ACE2 and TMPRSS2 and is blocked by a clinically proven protease inhibitor, Cell 181 (2) (2020) 271–280.e8, https://doi.org/10.1016/j.cell.2020.02.052.

[29] J. Lan, J. Ge, J. Yu, S. Shan, H. Zhou, S. Fan, Q.i. Zhang, X. Shi, Q. Wang, L. Zhang, X. Wang, Structure of the SARS-CoV-2 spike receptor-binding domain bound to the ACE2 receptor, Nature 581 (7807) (2020) 215–220, https://doi.org/10.1038/s41586-020-2180-5.

[30] J. Shang, G. Ye, K.e. Shi, Y. Wan, C. Luo, H. Aihara, Q. Geng, A. Auerbach, F. Li, Structural basis of receptor recognition by SARS-CoV-2, Nature 581 (7807) (2020) 221–224, https://doi.org/10.1038/s41586-020-2179-y.

[31] T.E. Tallei, S.G. Tumilaar, N.J. Niode, Fatimawali, B.J. Kepel, R. Idroes, Y. Effendi, S.A. Sakib, T.B. Emran, Potential of plant bioactive compounds as SARS-CoV-2 main protease (M(pro)) and Spike (S) glycoprotein inhibitors: a molecular docking study, Scientifica (Cairo) 2020 (2020) 6307457, https://doi.org/10.1155/2020/6307457.

[32] A.C. Pushkaran, P. Nath EN, A.R. Melge, R. Puthiyedath, C.G. Mohan, A phytochemical-based medication search for the SARS-CoV-2 infection by molecular docking models towards spike glycoproteins and main proteases, RSC Adv. 11 (20) (2021) 12003–12014, https://doi.org/10.1039/D0RA10458B.

[33] N. Thangavel, M.AI Bratty, H.A.AI Hazmi, A. Najmi, R.O.A. Alaqi, Molecular docking and molecular dynamics aided virtual search of olivenet directory for secoiridoids to combat SARS-CoV-2 infection and associated hyperinflammatory responses, Front. Mol. Biosci. 7 (2020) 627767, https://doi.org/10.3389/fmolb.2020.627767.

[34] S.K. Sinha, A. Shakya, S.K. Prasad, S. Singh, N.S. Gurav, R.S. Prasad, S.S Gurav, An *in-silico* evaluation of different Saikosaponins for their potency against SARS-CoV-2 using NSP_{15} and fusion spike glycoprotein as targets, J. Biomol. Struct. Dyn. 39 (9) (2021) 3244–3255, https://doi.org/10.1080/07391102.2020.1762741.

[35] R. Suravajhala, A. Parashar, G. Choudhir, A. Kumar, B. Malik, V.A. Nagaraj, G. Padmanaban, R. Polavarapu, P. Suravajhala, P.B.K. Kishor, Molecular docking and dynamics studies of curcumin with COVID-19 proteins, Netw. Model Anal. Health Inform. Bioinform. 10 (1) (2021), https://doi.org/10.1007/s13721-021-00312-8.

[36] A. Subbaiyan, K. Ravichandran, S.V. Singh, M. Sankar, P. Thomas, K. Dhama, Y. S. Malik, R.K. Singh, P. Chaudhuri, In silico molecular docking analysis targeting SARS-CoV-2 spike protein and selected herbal constituents, J. Pure Appl. Microbiol. 14 (suppl 1) (2020) 989–998, https://doi.org/10.22207/JPAM.14.SPL1.37.

[37] S. Maiti, A. Banerjee, Epigallocatechin gallate and theaflavin gallate interaction in SARS-CoV-2 spike-protein central channel with reference to the hydroxychloroquine interaction: bioinformatics and molecular docking study, Drug Dev. Res. 82 (1) (2021) 86–96, https://doi.org/10.1002/ddr.21730.

[38] A. Basu, A. Sarkar, U. Maulik, Molecular docking study of potential phytochemicals and their effects on the complex of SARS-CoV2 spike protein and human ACE2, Sci. Rep. 10 (1) (2020) 17699, https://doi.org/10.1038/s41598-020-74715-4.

[39] A. Ubani, F. Agwom, O.R. Morenikeji, S. Nathan, P. Luka, U.U. Umar, N.E. S. OmaleNnadi, J.C. Aguiyi, Molecular docking analysis of some phytochemicals on two SARS-CoV-2 targets: potential lead compounds against two target sites of SARS-CoV-2 obtained from plants, bioRxiv (2020), https://doi.org/10.1101/2020.03.31.017657.

[40] C.N. Patel, D. Goswami, D.G. Jaiswal, R.M. Parmar, H.A. Solanki, H.A. Pandya, Pinpointing the potential hits for hindering interaction of SARS-CoV-2 S-protein with ACE2 from the pool of antiviral phytochemicals utilizing molecular docking and molecular dynamics (MD) simulations, J. Mol. Graph. Model. 105 (2021) 107874, https://doi.org/10.1016/j.jmgm.2021.107874.

[41] G.Y. Chen, T.Y. Yao, A. Ahmed, Y.C. Pan, J.C. Yang, Y.C. Wu, The discovery of potential natural products for targeting SARS-CoV-2 spike protein by virtual screening, bioRxiv (2020), https://doi.org/10.1101/2020.06.25.170639.

[42] A.G. Al-Sehemi, F.A. Olotu, S. Dev, M. Pannipara, M.E. Soliman, S. Carradori, B. Mathew, Natural products database screening for the discovery of naturally occurring SARS-Cov-2 spike glycoprotein blockers, ChemistrySelect 5 (42) (2020) 13309–13317, https://doi.org/10.1002/slct.202003349.

[43] K. Gopinath, E.M. Jokinen, S.T. Kurkinen, O.T. Pentikäinen, Screening of natural products targeting SARS-CoV-2–ACE2 receptor interface – a MixMD based HTVS pipeline, Front. Chem. 8 (2020), https://doi.org/10.3389/fchem.2020.589769.

[44] J.A. Rothwell, et al., Phenol-Explorer 3.0: a major update of the Phenol-Explorer database to incorporate data on the effects of food processing on polyphenol content, Database (Oxford) 2013 (2013) bat070.

[45] V. Ruiz-Torres, J. Encinar, M. Herranz-López, A. Pérez-Sánchez, V. Galiano, E. Barrajón-Catalán, V. Micol, An updated review on marine anticancer compounds: the use of virtual screening for the discovery of small-molecule cancer drugs, Molecules 22 (7) (2017) 1037, https://doi.org/10.3390/molecules22071037.

[46] T. Sterling, J.J. Irwin, ZINC 15–ligand discovery for everyone, J. Chem. Inf. Model. 55 (11) (2015) 2324–2337, https://doi.org/10.1021/acs.jcim.5b00559.

[47] P. Banerjee, J. Erehman, B.O. Gohlke, T. Wilhelm, R. Preissner, M. Dunkel, Super Natural II–a database of natural products, Nucl. Acids Res. 43 (Database issue) (2015) D935–9, https://doi.org/10.1093/nar/gku886.

[48] D.S. Wishart, C. Knox, A.C. Guo, R. Eisner, N. Young, B. Gautam, D.D. Hau, N. Psychogios, S. Bouatra, R. Mandal, I. Sinelnikov, J. Xia, L. Jia, J.A. Cruz, E. Lim, C.A. Sobsey, S. Shrivastava, P. Huang, P. Liu, L. Fang, J. Peng, R. Fradette, D. Cheng, D. Tzur, M. Clements, A. Lewis, A.D. Souza, A. Zuniga, M. Dawe, Y. Xiong, D. Clive, R. Greiner, A. Nazyrova, R. Shaykhutdinov, L. Li, H.J. Vogel, I. Forsythe, HMDB: a knowledgebase for the human metabolome, Nucl. Acids Res. 37 (Database issue) (2009) D603–10, https://doi.org/10.1093/nar/gkn810.

[49] O. Trott, A.J. Olson, AutoDock Vina: improving the speed and accuracy of docking with a new scoring function, efficient optimization, and multithreading, J. Comput. Chem. 31 (2) (2010) 455–461, https://doi.org/10.1002/jcc.21334.

[50] S. Dallakyan, A.J. Olson, Small-molecule library screening by docking with PyRx, Methods Mol. Biol. 1263 (2015) 243–250, https://doi.org/10.1007/978-1-4939-2269-7_19.

[51] The PyMOL Molecular Graphics System Version 2.3.5. 2019, Schrödinger, LLC.

[52] Marvin Suite 6.0. ChemAxon.

[53] N.M. O'Boyle, M. Banck, C.A. James, C. Morley, T. Vandermeersch, G. R. Hutchison, Open Babel: an open chemical toolbox, J. Cheminf. 3 (1) (2011), https://doi.org/10.1186/1758-2946-3-33.

[54] R.A. Laskowski, M.B. Swindells, LigPlot+: multiple ligand-protein interaction diagrams for drug discovery, J. Chem. Inf. Model. 51 (10) (2011) 2778–2786, https://doi.org/10.1021/ci200227u.

[55] T. Sandar, OSIRIS Property Explorer [cited 2020 Nov 10]. Available from: https://www.organic-chemistry.org/prog/peo/.

[56] F. Tea, A. Ospina Stella, A. Aggarwal, D. Ross Darley, D. Pilli, D. Vitale, V. Merheb, F.X.Z. Lee, P. Cunningham, G.J. Walker, C. Fichter, D.A. Brown, W.D. Rawlinson, S. R. Isaacs, V. Mathivanan, M. Hoffmann, S. Pöhlman, O. Mazigi, D. Christ, D. E. Dwyer, R.J. Rockett, V. Sintchenko, V.C. Hoad, D.O. Irving, G.J. Dore, I. B. Gosbell, A.D. Kelleher, G.V. Matthews, F. Brilot, S.G. Turville, SARS-CoV-2 neutralizing antibodies: longevity, breadth, and evasion by emerging viral variants, PLoS Med. 18 (7) (2021) e1003656, https://doi.org/10.1371/journal.pmed.1003656.

[57] O. Sperandio, C.H. Reynès, A.-C. Camproux, B.O. Villoutreix, Rationalizing the chemical space of protein-protein interaction inhibitors, Drug Discov. Today 15 (5–6) (2010) 220–229, https://doi.org/10.1016/j.drudis.2009.11.007.

[58] S.-C. Gobeil, K. Janowska, S. McDowell, K. Mansouri, R. Parks, V. Stalls, M.F. Kopp, K. Manne, D. Li, K. Wiehe, K.O. Saunders, R.J. Edwards, B. Korber, B.F. Haynes, R. Henderson, P. Acharya, Effect of natural mutations of SARS-CoV-2 on spike structure, conformation, and antigenicity, Science 373 (6555) (2021), https://doi.org/10.1126/science:abi6226.

[59] J. Lyu, S. Wang, T.E. Balius, I. Singh, A. Levit, Y.S. Moroz, M.J. O'Meara, T. Che, E. Algaa, K. Tolmachova, A.A. Tolmachev, B.K. Shoichet, B.L. Roth, J.J. Irwin, Ultra-large library docking for discovering new chemotypes, Nature 566 (7743) (2019) 224–229, https://doi.org/10.1038/s41586-019-0917-9.

[60] M. Sorokina, C. Steinbeck, Review on natural products databases: where to find data in 2020, J. Cheminform. 12 (1) (2020) 20, https://doi.org/10.1186/s13321-020-00424-9.

[61] C. Gorgulla, A. Boeszoermenyi, Z.-F. Wang, P.D. Fischer, P.W. Coote, K. M. Padmanabha Das, Y.S. Malets, D.S. Radchenko, Y.S. Moroz, D.A. Scott, K. Fackeldey, M. Hoffmann, I. Iavniuk, G. Wagner, H. Arthanari, An open-source drug discovery platform enables ultra-large virtual screens, Nature 580 (7805) (2020) 663–668, https://doi.org/10.1038/s41586-020-2117-z.

[62] N. Murgolo, A.G. Therien, B. Howell, D. Klein, K. Koeplinger, L.A. Lieberman, G. C. Adam, J. Flynn, P. McKenna, G. Swaminathan, D.J. Hazuda, D.B. Olsen, T. C. Hobman, SARS-CoV-2 tropism, entry, replication, and propagation: considerations for drug discovery and development, PLoS Pathog. 17 (2) (2021) e1009225, https://doi.org/10.1371/journal.ppat.1009225.

[63] R.J. Bienstock, Computational drug design targeting protein-protein interactions, Curr. Pharm. Des. 18 (9) (2012) 1240–1254, https://doi.org/10.2174/138161212799436449.

[64] B.J. Bender, S. Gahbauer, A. Luttens, J. Lyu, C.M. Webb, R.M. Stein, E.A. Fink, T. E. Balius, J. Carlsson, J.J. Irwin, B.K. Shoichet, A practical guide to large-scale docking, Nat. Protoc. 16 (10) (2021) 4799–4832, https://doi.org/10.1038/s41596-021-00597-z.

[65] Y. Guo, L. Huang, G. Zhang, Y. Yao, H. Zhou, S. Shen, B. Shen, B. Li, X. Li, Q. Zhang, M. Chen, D. Chen, J. Wu, D. Fu, X. Zeng, M. Feng, C. Pi, Y. Wang, X. Zhou, M. Lu, Y. Li, Y. Fang, Y.Y. Lu, X. Hu, S. Wang, W. Zhang, G. Gao, F. Adrian, Q. Wang, F. Yu, Y. Peng, A.G. Gabibov, J. Min, Y. Wang, H. Huang, A. Stepanov, W. Zhang, Y. Cai, J. Liu, Z. Yuan, C. Zhang, Z. Lou, F. Deng, H. Zhang, C. Shan, L. Schweizer, K. Sun, Z. Rao, A SARS-CoV-2 neutralizing antibody with extensive Spike binding coverage and modified for optimal therapeutic outcomes, Nat. Commun. 12 (1) (2021) 2623, https://doi.org/10.1038/s41467-021-22926-2.